nature genetics

Mutations affecting the secretory COPII coat component SEC23B cause congenital dyserythropoietic anemia type II

Klaus Schwarz[1,2,14], Achille Iolascon[3,14], Fatima Verissimo[4], Nikolaus S Trede[5,6], Wyatt Horsley[5,6], Wen Chen[7], Barry H Paw[7], Karl-Peter Hopfner[8], Karlheinz Holzmann[9], Roberta Russo[3], Maria Rosaria Esposito[3], Daniela Spano[3], Luigia De Falco[3], Katja Heinrich[1], Brigitte Joggerst[4], Markus T Rojewski[1,2], Silverio Perrotta[10], Jonas Denecke[11], Ulrich Pannicke[1], Jean Delaunay[12], Rainer Pepperkok[4] & Hermann Heimpel[13]

Congenital dyserythropoietic anemias (CDAs) are phenotypically and genotypically heterogeneous diseases[1–4]. CDA type II (CDAII) is the most frequent CDA. It is characterized by ineffective erythropoiesis and by the presence of bi- and multinucleated erythroblasts in bone marrow, with nuclei of equal size and DNA content, suggesting a cytokinesis disturbance[5]. Other features of the peripheral red blood cells are protein and lipid dysglycosylation and endoplasmic reticulum double-membrane remnants[4,6]. Development of other hematopoietic lineages is normal. Individuals with CDAII show progressive splenomegaly, gallstones and iron overload potentially with liver cirrhosis or cardiac failure. Here we show that the gene encoding the secretory COPII component SEC23B is mutated in CDAII. Short hairpin RNA (shRNA)-mediated suppression of SEC23B expression recapitulates the cytokinesis defect. Knockdown of zebrafish *sec23b* also leads to aberrant erythrocyte development. Our results provide *in vivo* evidence for SEC23B selectivity in erythroid differentiation and show that SEC23A and SEC23B, although highly related paralogous secretory COPII components, are nonredundant in erythrocyte maturation.

We studied 33 individuals with congenital dyserythropoietic anemia type II (CDAII; MIM224100) from 28 unrelated families (**Supplementary Table 1**) of various ancestral backgrounds. CDAII was diagnosed on the basis of previously published criteria[7], including clinical aspects, bone marrow morphology and anomalous erythrocyte membrane proteins (**Supplementary Table 1**). In five families, the parents are consanguinous (F2, F6, F11, F16, F18). Assuming a recessive inheritance model, we conducted a screen for homozygous chromosomal regions using genome-wide SNP analysis for individuals F6P1 and F11P1. This analysis revealed a single common homozygous region on chromosome 20p11.23–20p12.1 (**Supplementary Table 2**), flanked by *KIF16B* on the telomeric side and *SLC24A3* on the centromeric side and encompassing 23 ORFs. The CDAII locus was originally mapped to 20q11 (ref. 8). In a refined contig build (build 36.3), the markers with the highest CDAII lod scores overlap the minimal homozygosity region on the short arm of chromosome 20 (ref. 9). The amalgamation of these results with the proposition of impaired *cis*, *medial* and *trans* *N*-glycan Golgi processing of erythroblast glycoproteins in CDAII[10] made secretory pathway components potential candidates. We therefore sequenced the *SEC23B* gene, which is located in the critical region and encodes a COPII component, in all 33 individuals. We detected 12 different missense mutations, five nonsense mutations, one single-nucleotide as well as one large deletion and one splice-site mutation (**Fig. 1a** and **Supplementary Table 3**). Seventeen individuals are compound heterozygotes, whereas 16 individuals, including the eight in the five consanguinous families, are homozygotes. Every case bears at least one missense mutation, suggesting that the presence of two severe mutations may be lethal. There are two hot spots of mutation, with 325G>A accounting for 30% (20 of 66 alleles) and 40C>T for 15% (10 of 66 alleles) of the mutations. Haplotype analyses failed to demonstrate the existence of a founder effect (data not shown). When data on parents were available, we found that parents were heterozygous for the mutations, excluding the occurrence of *de novo* mutations in these

[1]Institute for Transfusion Medicine, University of Ulm, Ulm, Germany. [2]Institute for Clinical Transfusion Medicine and Immunogenetics Ulm, German Red Cross Blood Service Baden-Wuerttemberg-Hessen, Ulm, Germany. [3]Department of Biochemistry and Medical Biotechnologies, University Federico II of Naples and CEINGE Advanced Biotechnologies, Naples, Italy. [4]Cell Biology and Biophysics, European Molecular Biology Laboratory, Heidelberg, Germany. [5]Huntsman Cancer Institute and [6]Department of Pediatrics, University of Utah, Salt Lake City, Utah, USA. [7]Department of Medicine, Hematology Division, Brigham & Women's Hospital, and Hematology-Oncology Division, Children's Hospital Boston, Harvard Medical School, Boston, Massachusetts, USA. [8]Center for Integrated Protein Science and Gene Center, Department of Chemistry and Biochemistry, Ludwig-Maximilians-University Munich, Munich, Germany. [9]Chip Facility ZKF, University Hospital Ulm, Ulm, Germany. [10]Department of Pediatrics, Second University of Naples, Naples, Italy. [11]Department of Pediatrics, University of Rostock, Rostock, Germany. [12]INSERM U 779, Hôpital de Bicêtre, 94275 Le Kremlin-Bicêtre, France. [13]Department Internal Medicine III, University Hospital Ulm, Ulm, Germany. [14]These authors contributed equally to this work. Correspondence should be addressed to K.S. (klaus.schwarz@uni-ulm.de) or A.I. (iolascon@ceinge.unina.it).

Received 12 March; accepted 1 June; published online 28 June 2009; doi:10.1038/ng.405

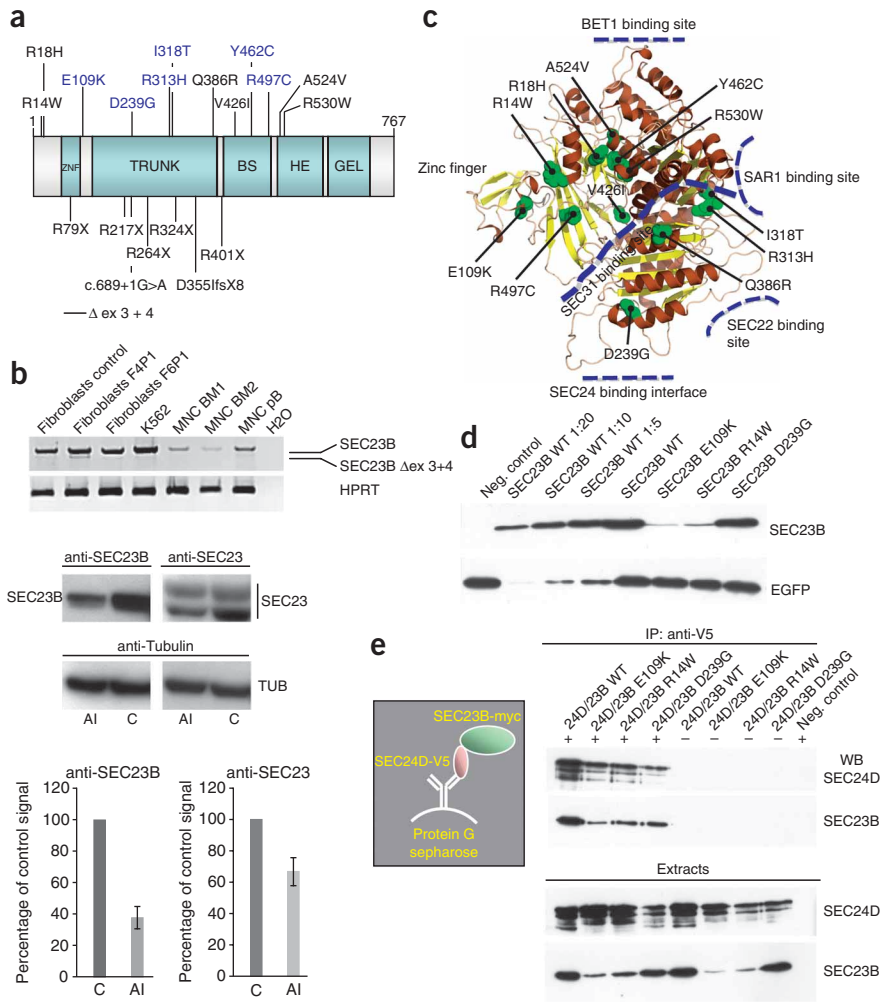

Figure 1 *SEC23B* mutation analysis. (**a**) *SEC23B* mutations are projected on the schematic domain structure of SEC23B. Mutations are indicated in blue when detected in more than one kindred. (**b**) Upper panel shows SEC23B RT-PCR of normal and two affected individuals (F4P1, F6P1) fibroblasts, K562 cells and normal mononuclear cells (MNC) of bone marrow (BM) and peripheral blood (pB). (For BM2, only 20% of RNA was used as compared to the other analyses. For MNC BM1, MNC BM2 and MNC pB, the gel loading was doubled.) Lower panels show quantity of SEC23B and total SEC23 protein as analyzed by protein blot in a control (C) and an affected individual (AI) cell line (F4P1). Quantification of three independent experiments shows that the patient cell line has 38% ± 7% of SEC23B compared to control. Total SEC23 is 67% ± 9% of control. Tubulin detection was used as loading control. (**c**) Model of human SEC23B shown as ribbon plot with highlighted secondary structure. The model was generated on the basis of the crystal structure of human SEC23A. The side chains of mutated residues in SEC23B are shown as green spheres. Binding sites for known interaction partners are indicated[16,23–25]. (**d**) Dilution analysis of SEC23B wild-type and mutants overexpressed after transient transfections in HEK293T cells. The EGFP signal is for the transfection and loading control. (**e**) Coimmunoprecipitation of SEC23B wild-type and mutants. The presence (+) or absence (−) of the antibody to V5 is indicated.

individuals and supporting autosomal recessive inheritance (**Supplementary Table 3**). The mutations affect most domains of SEC23B; only the C-terminal gelsolin-like domain is spared (**Fig. 1a**). All missense mutations affect highly conserved residues (**Supplementary Table 4**). From our analyses, we conclude that most individuals with CDAII bear *SEC23B* mutations.

In healthy subjects, the mutation 790C>T was heterozygously detected once in 237 individuals, and the substitution 276G>A was present heterozygously 24 times in 354 subjects (6.7%). Changes present more than once in the cohort were not detected in at least 237 healthy individuals; sporadic mutations were never seen on 200 chromosomes of healthy subjects.

SEC23B missense mutations of F4P1 and F6P1 showed no gross influence on *SEC23B* RNA stability (**Fig. 1b**). In contrast, the F4P1 RNA with the exon 3+4 deletion was barely detectable, possibly owing to a frameshift and premature stop codon resulting in nonsense-mediated decay (**Fig. 1b**). We observed normal *SEC23B* RNA expression in peripheral blood of F20P1 and F26P1 by RT-PCR (data not shown). No alternative *SEC23B* splice products were detectable in mononuclear cells of bone marrow and blood, K562 erythroleukemic cells and normal dermal fibroblasts (**Fig. 1b**).

By protein blotting, we quantified with different polyclonal antibodies SEC23B and total SEC23 (A and B) proteins in control and F4P1 fibroblasts (**Fig. 1b**). Evaluation of three independent experiments showed that the cell line of the affected individual had 38% ± 7% of SEC23B, and total SEC23 was 67% ± 9% when normalized to the 100% in the control.

The secretory pathway in eukaryotic cells is critical for membrane homeostasis, localization of proteins within cells and secretion of extracellular factors. During a budding reaction, cytoplasmic coat proteins (COPs) are assembled on a membrane surface, capture cargo molecules and polymerize into a cage sculpting different-sized cargo vesicles. In yeast, COPII-coated vesicles form by the sequential binding of Sar1-GTP, the inner complex proteins Sec23–Sec24 and the outer complex components Sec13–Sec31 on the endoplasmic reticulum (ER)[11,12]. Sec23–Sec24 is implicated in selective cargo sorting destined for the *cis*-Golgi apparatus but has additional roles in completion of the coat assembly, tethering of vesicles to their targets and regulating traffic[13]. For Sec23, additional roles in autophagy and in receptor internalization have been claimed[14,15].

To analyze potential mechanistic consequences of the identified missense mutations, we generated a model of human SEC23B (**Fig. 1c**) on the basis of the highly related (**Supplementary Table 4**) human SEC23A crystal structure[16]. Mutations severely truncating SEC23B are unlikely to give a soluble, stable and folded peptide. R18H, V426I, Y462C, A524V and R530W are located in or near the core structures of SEC23B. These mutations might destabilize the protein or perturb the fold. R14W, E109K and R497C are located in the zinc-finger domain or at its interface with other domains. These mutations likely disrupt the function or orientation of the zinc-finger domain or may affect protein-protein interactions. D239G is situated near the SEC24 binding site and may interfere with proper SEC24 interaction. R313H and I318T are near the SAR1 binding site in a region where SEC31 also binds. These mutations could perturb

interaction with SAR1 and/or SEC31. Finally, Q386R is located near the SEC31 binding groove and likely interferes with SEC31 binding.

For protein studies, we selected one zinc-finger domain (E109K) mutant and one mutant situated at the interface of the zinc-finger domain and SEC23B core fold (R14W) (both together account for about 50% of the mutations) as well as the mutant D239G, which is situated near the SEC24 binding site. Overexpression of C-terminally tagged SEC23B mutants by transient transfection in HEK293T cells revealed the instability of the zinc-finger–associated mutants, with less than 5% of protein detectable compared to wild-type SEC23B (**Fig. 1d**), supporting the results of primary fibroblast analyses. The D239G mutation did not impair SEC23B stability (**Fig. 1d**).

To unravel potential functional consequences of the three mutant proteins, we carried out coimmunoprecipitation experiments with V5-C-terminally labeled SEC24D, a SEC24 isoform previously implicated in SEC23A binding[17]. All three mutants (E109K, R14W and D239G) were coimmunoprecipitated by SEC24D with similar SEC23B/SEC24D ratios as in crude cell extracts (**Fig. 1e**), implying that the overall structure and the SEC23B–SEC24D interface of the mutants is not disordered. Similar results were obtained with SEC24C (data not shown).

Why does impairment of SEC23B lead to such a specific erythropoietic phenotype, considering its central role in secretion? In humans, two SEC23 isoforms, SEC23A and SEC23B, have been noted. We suspected that the CDAII phenotype may be caused by tissue-specific expression of SEC23A versus SEC23B. We observed no gross RNA expression difference between the paralogs in primary dermal fibroblasts (data not shown). When *in vitro* erythroid differentiation of $CD34^+$ blood cells was conducted for 7–14 d, *SEC23B* RNA expression increased 5–7 fold over *SEC23A* RNA expression (**Fig. 2a**), whereas in the seeded $CD34^+$ cells, the relative expression levels were equal. Protein blot analysis revealed an increased amount of SEC23B protein in $CD34^+$ blood cells 14 d after differentiation initiation as compared to 7 d (**Fig. 2a**). We did not analyze SEC23A at the protein level because we lacked a suitable specific antibody.

To imitate SEC23B protein reduction in individuals with CDAII and to elucidate the functional role of SEC23B downregulation, we generated stable pools of the erythroleukemic cell line K562 after transfection with a translation-interfering SEC23B-silencing shRNA-mir vector and control vectors. We observed no difference of *SEC23B* RNA expression in silenced and nonsilenced K562 pools (**Fig. 2b**). SEC23B protein expression in SEC23B-silenced K562 pools was 44.8% compared to K562, and 64.0% compared to the nonsilenced shRNA-mir pools (**Fig. 2b**). After SEC23B silencing of K562, FACS cell cycle analysis showed a threefold increase of the percentage of cells in the G2+M phase (that is, cells containing twice the amount of DNA) over controls ($P = 0.02$) (**Fig. 2c**). This observation prompted the question of whether the increased percentage of cells with double DNA content may be in part due to binucleated cells. Microscopy of stable pools stained with 4,6-diamidino-2-phenylindole (DAPI) showed the

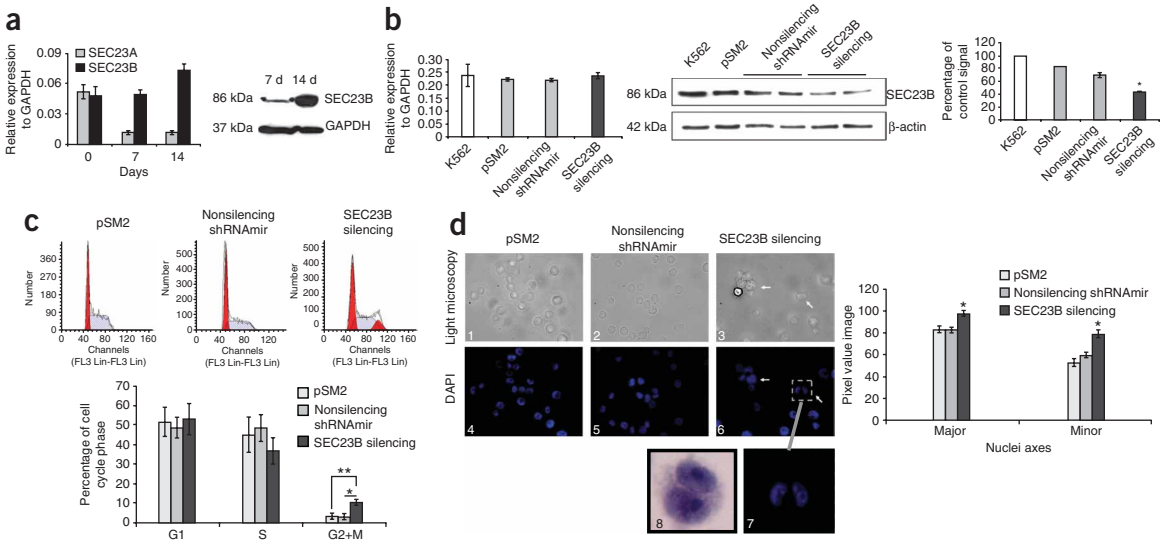

Figure 2 SEC23B expression and function in erythroid cells. (**a**) Left panel shows gene expression analyses of *SEC23A* and *SEC23B* during *in vitro* erythroid differentiation of peripheral blood $CD34^+$ cells from healthy controls as assessed by qRT-PCR. At 7 d after erythropietin (EPO) treatment, *SEC23B* showed an increased expression (0.05 ± 0.004, mean ± s.d) compared with *SEC23A* gene expression (0.01 ± 0.002; $P = 0.0001$, Student's *t*-test). This difference is more visible 14 d after differentiation (*SEC23B* 0.07 ± 0.006 versus *SEC23A* 0.01 ± 0.002, $P = 0.0001$, Student's *t*-test). Right panel shows protein blot analysis of SEC23B expression during *in vitro* erythroid differentiation of peripheral blood $CD34^+$ cells from healthy controls. (**b**) Left panel shows *SEC23B* RNA expression analysis of K562 stable pools. No significant variation in SEC23B-silenced cells was observed when compared to the controls (mean ± s.d.). Right panels show SEC23B protein expression in K562 stable pools. Decreased protein expression in K562 stable pools silenced for SEC23B is 55.2% compared to K562 wild-type, and 36.0% compared to K562 treated with nonsilencing shRNAmir (*$P = 0.03$; Student's *t*-test). (**c**) Cell cycle analyses of K562 stable pools (one of three experiments). The black line shows all detected cells, the high red peak represents the cells in G0+G1 phases, the hatched area are the cells in S phase and the low red peak are the cells in G2+M phases. The diagram summarizes triplicate results for each cell cycle phase (mean ± s.e.m.). A significant increase of the cell percentage silenced for SEC23B in the G2+M phase (10.3% ± 1.4) when compared to control stable pools (pSM2, 3.2% ± 1.7, **$P = 0.02$; nonsilencing shRNAmir, 2.9% ± 1.7, *$P = 0.02$; Student's *t*-test) was observed. (**d**) Microscopic analysis of K562 stable pools with the presence of binucleated cells in SEC23B-silenced cells after DAPI (indices 3, 6, 7) or hematoxylin-eosin (index 8) staining. Comparison of the nuclei major and minor axes between control pools and SEC23B-silenced K562 pool. Detection of an increased major axis in silenced cells (97.8 ± 2.3 pixels) compared to PSM2 cells (83.1 ± 2.8, $P = 0.0002$) and to nonsilenced cells (82.8 ± 2.4, $P = 0.0001$) (Student's *t*-test) and an increased minor axis in silenced cells (78.7 ± 3.5 pixels) compared to PSM2 cells (53.1 ± 3.4, $P = 0.00001$) and to nonsilenced cells (59.6 ± 2.4, $P = 0.0001$) (Student's *t*-test). Data are shown as mean ± s.e.m.

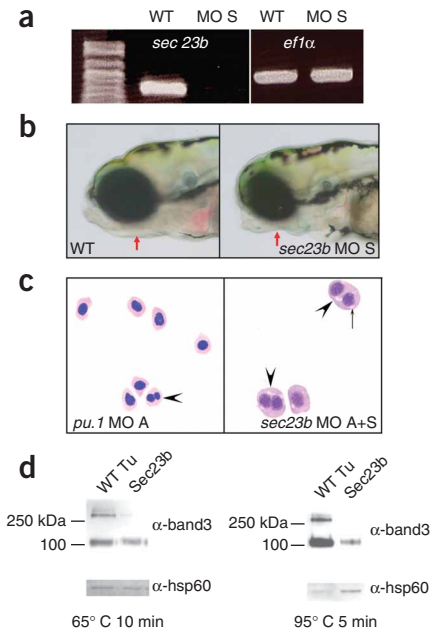

Figure 3 Analysis of *sec23b* zebrafish morphants. (**a**) Absence of wild-type *sec23b* transcript in *sec23b* splice-blocking morphants. Embryos were either left untreated (WT) or were injected at the 1- to 8-cell stage with *sec23b* splice-blocking morpholino (MO S). (**b**) Brightfield images of wild-type (WT) and *sec23b* MO S morphants obtained at 3 d.p.f. Red arrows indicate lower jaw. Note the reduced jaw morphology in morphants compared to WT. Magnification is ×100. (**c**) Erythrocytes from *pu.1* and *sec23b* MO A+S morphants obtained at 3 d.p.f. Arrowheads point to binucleated erythrocytes. Note immaturity, large size and perinuclear lucency (black arrow) of *sec23b* morphant erythrocytes. Magnification is ×100. A, translation blocking MO; S, splice blocking MO; A+S, translation and splice blocking MO. (**d**) Absence of structural differences of erythrocyte band3 (slc4a1) from control and *sec23b* morphant embryos. Red blood cells were denatured for either 65 °C or for 95 °C . Western blot was performed using anti-zebrafish band3 antisera. Aggregates of band3 proteins were noted at higher molecular weight irrespective of denaturation temperatures. As a loading control, the same PVDF membrane was reprobed with anti-hsp60.

presence of binucleated cells in SEC23B-silenced K562 cells (**Fig. 2d**, indices 3, 6, 7); no binucleated cells were present in controls (**Fig. 2d**, indices 1, 4 and 2, 5). Hematoxylin-eosin staining confirmed the presence of binucleated cells (**Fig. 2d**, index 8). The major and minor axes of SEC23B-silenced K562 nuclei were significantly increased in size (**Fig. 2d**). These results support the hypothesis that the cell cycle of erythroid cells and their cytokinesis depend on a sufficient level of SEC23B.

To independently confirm the function of SEC23B in erythrocyte development, we examined its role in zebrafish embryos using antisense morpholino technology. The *sec23b* and the *pu.1* translation-blocking morpholinos[18,19] were previously described. Efficacy of the *sec23b* intron 4 splice donor–blocking morpholino (MO S) was verified by RT-PCR (**Fig. 3a**). Injection of the *sec23b* translation-blocking morpholino (MO A at 4 ng; data not shown) and the *sec23b* MO S (1 ng, **Fig. 3b**) led to a pronounced reduction of the lower jaw on day 3 post fertilization (d.p.f.) as observed previously in *sec23b* and *sec23a* morphants[18,20]. Injection of a *pu.1* translation-blocking morpholino (4 ng) had no effect (data not shown). Given the observation of the redundant function of SEC23A and SEC23B in the maintenance of ERES and secretion of cargo, these findings must be dissected in future experiments.

Erythrocytes from wild-type and *pu.1* morphants were age-appropriate on 3 d.p.f. and showed less than 0.2% (**Table 1**) well-differentiated binucleated cells (**Fig. 3c**). However, erythrocytes in *sec23b* morphants appeared larger, and we detected a significant increase in immature, binucleated erythrocytes (**Table 1** and **Fig. 3c**) similar to that in human individuals with CDAII. We also explored hypoglycosylation of band3, another hallmark of mature erythrocytes of CDAII-affected individuals, in *sec23b* zebrafish morphants. Although we observed underexpression of band3 in morphants, we found no evidence of N-linked hypoglycosylation of band3 (**Fig. 3d**). Finally, duplication of rough ER, another CDAII characteristic, was not seen in zebrafish erythrocytes with transmission electron microscopy (data not shown). The *sec23a* mutant zebrafish line *crusher* showed normal erythrocyte development (data not shown). These observations are consistent with the idea that SEC23B has an evolutionarily conserved function in erythrocyte development. The failure to recapitulate the complete human phenotype in zebrafish *sec23b* morphants may be due to lethality at 6 d.p.f.; morphant erythropoiesis had to be scored at the larval stage with primitive wave erythropoiesis while the erythroblasts from individuals with CDAII are definitive wave hematopoiesis. We can speculate that the two different programs have a differential requirement for *sec23b* such as has been observed for many cytoskeletal membrane proteins (band3, protein4.1 or β-spectrin).

Additional experiments (**Supplementary Note**) underscore the erythrocyte specificity of SEC23B deficiency and the redundant function of human SEC23A and SEC23B in cells (fibroblasts, HeLa cells) other than the erythroid lineage (**Supplementary Figs. 1** and **2**). Alternatively, the cargo proteins carried by COPII vesicles may differ between fibroblasts and HeLa cells versus erythroblasts, explaining the lack of an obvious phenotype in these cells.

In conclusion, we have shown that mutations in *SEC23B* cause CDAII. In some cases, a reduction in SEC23B expression occurs, which in erythroblasts may not be sufficiently compensated for by SEC23A

Table 1 Statistical analyses of jaw phenotype and erythroid binuclearity in wild-type and morphant zebrafish

Evaluation of jaw morphology in morphants at 72 h.p.f.

		Number of embryos		
Type of embryo		Normal	Abnormal	*P* value[a]
Wild type		97	11	
sec23b MOS	1 ng	0	175	<0.0001
Pu.1 MO A	4 ng	88	12	0.8254

Evaluation of erythrocyte binuclearity in morphants at 72 h.p.f.

	Number of erythrocytes counted			
Type of embryo	Mononuclear	Binuclear	%	*P* value[a]
Wild type	3,286	6	0.18	
sec23b MO S 1 ng	973	11	1.11	0.0004
sec23b MO A+S[b]	1,870	38	2.03	<0.0001
pu.1 MO A 4 ng	1,442	2	0.14	0

h.p.f., hours post fertilization.
[a]Comparing the number of embryos of the total with severe jaw phenotype or binuclearity (Fisher exact test, two-tailed). [b]To obtain maximal inhibition of Sec23 protein expression, embryos were injected with a mixture of MO A (4 ng) and MO S (1 ng) (MO A+S).

and thus may result in erythrocyte-specific defects in COPII-mediated ER export, ultimately leading to the clinical and cellular phenotype.

Incomplete cytokinesis is one of the key features of CDAII erythrocytes. The midbody is a transient 'organelle-like' structure remnant of cell division just before abscission. SEC23B was identified in a screen for midbody components[21]. Whether SEC23B plays an active role in erythrocyte midbody assembly or deconstruction or whether glycosylation impairment indirectly affects cytokinesis remains to be established.

Mutations in genes encoding three COPII components have been assigned to human genetic disorders. *SAR1B* defects cause the chylomicron retention disease, Anderson disease and Marinesco-Sjogren syndrome, resulting in lipid malabsorption[22]. *SEC23A* is mutated in cranio-lenticulo-sutural dysplasia leading to skeletal developmental defects[17,20]. *SEC23B* impairment is the basis of CDAII. These studies are consistent with the hypothesis that COPII components may act as membrane-coating modules with cargo selectivity. Delineating additional genetic diseases caused by defects in COPII components may help identify developmental and cell type–specific tasks of each individual isoform of this secretory structure.

METHODS

Methods and any associated references are available in the online version of the paper at http://www.nature.com/naturegenetics/.

Accession codes. GenBank: RefSeq *SEC23B* DNA, NM_006363; RefSeq SEC23B peptide, NP_006354.

Note: Supplementary information is available on the Nature Genetics website.

ACKNOWLEDGMENTS

We acknowledge the technical assistance of S. Braun, I. Janz, T. Kersten, G. Baur, T. Becker and R. Leichtle. Anti-ts-O45-G monoclonal antibody 'VG' was a gift from K. Simons (Max Planck Institute of Molecular Cell Biology and Genetics). HeLa-Kyoto cells (human cervix carcinoma cells) were from S. Narumiya (Kyoto University) and T. Hirota (Institute of Molecular Pathology). These studies were supported by the German Red Cross Blood Service Baden-Wuerttemberg-Hessen to K.S., by the University of Ulm to H.H. and by the Else Kröner Fresenius Stiftung to K.S. and H.H. Additional support was provided by the Italian Ministero dell'Università e della Ricerca, by Telethon (Italy), by grants MUR-P35/126/IND and by grants Convenzione CEINGE-Regione Campania-Ass. Sanità to A.I. University of Utah Core facilities were supported by an US National Institutes of Health grant. K.-P.H. acknowledges support from the Deutsche Forschungsgemeinschaft (SFB 684). We thank the DIM Facility for imaging microscopy and the Flow Cytometry Facility for cell cycle analyses at CEINGE Institute.

AUTHOR CONTRIBUTIONS

K.S., A.I. and H.H. designed the study. H.H., A.I., S.P. and J. Delaunay treated subjects, collected clinical data and, together with J. Denecke, performed clinical laboratory analyses. K. Holzmann performed and K. Holzmann and K.S. analyzed the chip experiments. K.S., F.V., R.R., M.R.E., D.S., L.D.F., K. Heinrich, B.J., U.P. and R.P. performed the molecular, protein and cell analyses. K.-P.H. modeled the SEC23B structure. N.S.T. and W.H. performed zebrafish morpholino injections, blood cell preparations and electron microscopy. W.C. and B.H.P. performed the zebrafish western blot analysis. M.T.R. did the FACS analyses and fibroblast differentiation. K.S., A.I. and H.H. wrote the paper.

Published online at http://www.nature.com/naturegenetics/.
Reprints and permissions information is available online at http://npg.nature.com/reprintsandpermissions/.

1. Heimpel, H. & Wendt, F. Congenital dyserythropoietic anemia with karyorrhexis and multinuclearity of erythroblasts. *Helv. Med. Acta* **34**, 103–115 (1968).
2. Wickramasinghe, S.N. Congenital dyserythropoietic anemias. *Curr. Opin. Hematol.* **7**, 71–78 (2000).
3. Iolascon, A. Congenital dyserythropoietic anemias: a still unsolved puzzle. *Haematologica* **85**, 673–674 (2000).
4. Heimpel, H. & Iolascon, A. in *Disorders of Homeostasis, Erythrocytes, Erythropoiesis.* 1st edn (eds. Beaumont, C., Beris, P., Beuzard, Y. & Brugnara, C.) Congenital dyserythropoietic anemia 120–142 (European School of Haematology, Paris, 2006).
5. Queisser, W., Spiertz, E., Jost, E. & Heimpel, H. Proliferation disturbances of erythroblasts in congenital dyserythropoietic anemia type I and II. *Acta Haematol.* **45**, 65–76 (1971).
6. Iolascon, A. *et al.* Congenital dyserythropoietic anemia type II: molecular basis and clinical aspects. *Haematologica* **81**, 543–559 (1996).
7. Heimpel, H. *et al.* Congenital dyserythropoietic anemia type II: epidemiology, clinical appearance, and prognosis based on long-term observation. *Blood* **102**, 4576–4581 (2003).
8. Gasparini, P. *et al.* Localization of the congenital dyserythropoietic anemia II locus to chromosome 20q11.2 by genomewide search. *Am. J. Hum. Genet.* **61**, 1112–1116 (1997).
9. Denecke, J. & Marquardt, T. Congenital dyserythropoietic anemia type II (CDAII/HEMPAS): Where are we now? *Biochim. Biophys. Acta* advance online publication doi:10.1016/j.bbadis.2008.12.005 (25 December 2008).
10. Denecke, J. *et al.* Characterization of the N-glycosylation phenotype of erythrocyte membrane proteins in congenital dyserythropoietic anemia type II (CDA II/HEMPAS). *Glycoconj. J.* **25**, 375–382 (2008).
11. Lee, M.C., Miller, E.A., Goldberg, J., Orci, L. & Schekman, R. Bi-directional protein transport between the ER and Golgi. *Annu. Rev. Cell Dev. Biol.* **20**, 87–123 (2004).
12. Fromme, J.C., Orci, L. & Schekman, R. Coordination of COPII vesicle trafficking by Sec23. *Trends Cell Biol.* **18**, 330–336 (2008).
13. Cai, H., Reinisch, K. & Ferro-Novick, S. Coats, tethers, Rabs, and SNAREs work together to mediate the intracellular destination of a transport vesicle. *Dev. Cell* **12**, 671–682 (2007).
14. Ishihara, N. *et al.* Autophagosome requires specific early Sec proteins for its formation and NSF/SNARE for vacuolar fusion. *Mol. Biol. Cell* **12**, 3690–3702 (2001).
15. Penalver, E., Lucero, P., Moreno, E. & Lagunas, R. Clathrin and two components of the COPII complex, Sec23p and Sec24p, could be involved in endocytosis of the *Saccharomyces cerevisiae* maltose transporter. *J. Bacteriol.* **181**, 2555–2563 (1999).
16. Mancias, J.D. & Goldberg, J. The transport signal on Sec22 for packaging into COPII-coated vesicles is a conformational epitope. *Mol. Cell* **26**, 403–414 (2007).
17. Fromme, J.C. *et al.* The genetic basis of a craniofacial disease provides insight into COPII coat assembly. *Dev. Cell* **13**, 623–634 (2007).
18. Lang, M.R., Lapierre, L.A., Frotscher, M., Goldenring, J.R. & Knapik, E.W. Secretory COPII coat component Sec23a is essential for craniofacial chondrocyte maturation. *Nat. Genet.* **38**, 1198–1203 (2006).
19. Rhodes, J. *et al.* Interplay of pu.1 and gata1 determines myelo-erythroid progenitor cell fate in zebrafish. *Dev. Cell* **8**, 97–108 (2005).
20. Boyadjiev, S.A. *et al.* Cranio-lenticulo-sutural dysplasia is caused by a *SEC23A* mutation leading to abnormal endoplasmic-reticulum-to-Golgi trafficking. *Nat. Genet.* **38**, 1192–1197 (2006).
21. Skop, A.R., Liu, H., Yates, J. III., Meyer, B.J. & Heald, R. Dissection of the mammalian midbody proteome reveals conserved cytokinesis mechanisms. *Science* **305**, 61–66 (2004).
22. Jones, B. *et al.* Mutations in a Sar1 GTPase of COPII vesicles are associated with lipid absorption disorders. *Nat. Genet.* **34**, 29–31 (2003).
23. Bi, X., Corpina, R.A. & Goldberg, J. Structure of the Sec23/24-Sar1 pre-budding complex of the COPII vesicle coat. *Nature* **419**, 271–277 (2002).
24. Mossessova, E., Bickford, L.C. & Goldberg, J. SNARE selectivity of the COPII coat. *Cell* **114**, 483–495 (2003).
25. Bi, X., Mancias, J.D. & Goldberg, J. Insights into COPII coat nucleation from the structure of Sec23.Sar1 complexed with the active fragment of Sec31. *Dev. Cell* **13**, 635–645 (2007).

ONLINE METHODS

Subjects. Subjects were collated in the German Registry on CDAs in Ulm, Germany (F1 through F13) and the International Registry on CDAII in Naples, Italy (F14 through F28). The diagnosis was based on history, clinical findings, laboratory data, morphological analysis of aspirated bone marrow, evidence of defective band3 glycosylation shown by SDS-PAGE and/or on increased erythrocyte agglutination by antisera. In subjects F3P1 and F5P1, where SDS-PAGE was not available, the diagnosis was confirmed by positive acidified serum lysis test being specific for CDAII[26].

The subjects gave informed consent for the studies. Collation of subject data in the German Registry on CDAs and use of anonymized data and samples for research were permitted by the ethical committee of the University of Ulm.

Cell lines and cell culture. Human primary dermal fibroblasts were grown in Iscove's Modified Dulbecco's medium (IMDM, Gibco) supplemented with 10% FCS (PAA) at 37 °C and 7.5% CO_2. HEK-293T cells were cultivated in DMEM (Gibco) plus 10% FCS at 37 °C and 7.5% CO_2. K562 cells were grown in IMDM (Sigma) supplemented with 10% FBS, 2 mM L-glutamine (Euro-clone) and 1% (v/v) antibiotics (10,000 U/ml penicillin, and 10 mg/ml streptomycin (Euro-clone)) at 37 °C and 5% CO_2. For *in vitro* erythroid development, $CD34^+$ cells were isolated from the peripheral blood of nine healthy human controls divided in three pools and plated on plastic culture dishes in methylcellulose medium containing 3 U/ml erythropoietin (Janssen-Cilag) as previously described[27].

Genomic DNA preparation. Genomic DNA was prepared using the QIAamp DNA Blood Kit (Qiagen).

SNP-analysis and homozygosity determination. Genotyping was conducted on the Affymetrix GeneChip platform using the 50K Xba array of the Affymetrix 100K system, which consists of about 50,000 SNPs (Affymetrix). We subjected 250 ng of DNA to restriction endonuclease digestion by XbaI, followed by processing according to the manufacturer's instructions (see URLs section for complete protocol). Arrays were hybridized, stained, washed and scanned using a Hybridization Oven 640, Fluidics station FS450 and a GeneChip Scanner 3000 7G according to the instructions of the manufacturer. Genotying was conducted on the GTYPE Software 4.0 using the RLMM genotype-calling algorithm. Homozygous regions were detected using CNAT4.0 (Affymetrix) and visualized with the IdeogramBrowser.

Genomic sequencing. For *SEC23B* exon sequencing, we amplified and sequenced 100 ng genomic DNA (primers are available on request) with a Big Dye Terminator v1.1 Cycle Sequencing Kit (Applied Biosystems). Sequence products were separated on an Applied Biosystems Prism 3100C Genetic Analyzer.

RNA isolation and RT-PCR. RNA was isolated with the RNeasy Mini Kit (Qiagen) followed by DNase digestion. We reverse transcribed 1 µg total fibroblast RNA using the SuperScript II Reverse Transkriptase Kit (Invitrogen) with random hexamer priming. Primers and conditions are available on request.

qRT-PCR. Total cellular RNA was extracted by a method described previously[28]. We carried out the RT reactions using the iScript cDNA Synthesis Kit (BioRad), according to the manufacturer's instructions. Quantitative real-time qRT-PCR was performed using the SYBR Green PCR Master Mix (Applied Biosystems) with the Applied Biosystem Model 7900HT Sequence Detection System. Primers and conditions are available on request. Relative gene expressions were calculated by using the $2^{-\Delta Ct}$ method, as previously described[29]. The significance of the gene expression differences was determined using the Student's t test. A two-sided $P < 0.05$ was considered statistically significant.

Cloning of cDNA products into expression vectors. cDNA products were purified with QIAquick PCR Purification Kit (Qiagen), cloned into pcDNA6/myc-HIS- or pcDNA6/V5-HIS-vectors (Invitrogen) and transformed into the XL-2blue bacterial Strain (Stratagene). Plasmids were purified with the QIAprep Miniprep Kit (Qiagen) and sequenced with the primers used for generating the PCR products.

Transfection experiments. We nucleofected 2×10^6 HEK293T cells with a total of 5 µg expression plamids (2.25 µg pcDNA6/myc-HIS vector, 2.25 µg pcDNA6/V5-HIS-vector and 0.5 µg pEGFP-N1 vector) using Nucleofector Kit V (Lonza). Following 48 h of cultivation, cell extracts were harvested in lysis buffer (50 mM Tris pH 8.0, 62.5 mM EDTA, 1% Nonidet P-40 and 0.4% deoxycholate). We transfected 0.8×10^6 K562 cells with 2.5 µg Expression Arrest pSM2 retroviral shRNAmir plasmids (empty vector and nonsilencing vector as controls, and shRNAmir plasmid against SEC23B) (Open Biosystems) using TransIT-LT1 transfection reagent (Mirus). To select stable pools, 48 h after transfection, the cells were cultured under 2 µg/ml puromycin (Invitrogen). For sequence of shRNA, see **Supplementary Table 5**.

Coimmunoprecipitation experiments. After transfections, cell extracts were prepared in immunoprecipitation buffer (25 mM Hepes pH 7.4, 150 mM KCl, 10 mM $MgCl_2$, 10% glycerol, 0.1% Nonidet P-40, 2 mM DTT, and a protease inhibitor cocktail). We incubated 400 µg extract with mouse antibody to V5 (R950-25, Invitrogen) (30 min, 4 °C) in a final volume of 500 µl immunoprecipitation buffer followed by overnight incubation with Protein G Sepharose (GE Healthcare). Precipitates were washed three times in immunoprecipitation buffer before loading onto denaturing SDS gels.

Protein blotting. On an 8% SDS gel, 15 µg protein extract was loaded per lane. After separation, the proteins were blotted semidry on an Immobilon-P membrane (Millipore). First antibodies (mouse antibody to myc R950-25 or mouse antibody to V5 R960-25) were used as 1:5000 solutions; secondary goat anti-mouse antibodies coupled to horseradish peroxidase (HRP) were diluted 1:3000 (dilutions in: 10 mM Tris HCl pH 7.5, 150 mM NaCl, 0.05% Tween 20 and 5% milk powder). For SEC23B expression analysis of differentiated $CD34^+$ cells and K562 stable pools, a rabbit antibody to SEC23B (1:500; Sigma) was used. HRP-conjugated anti-rabbit antibody (1:10,000) (Santa Cruz Biotechnology) served as secondary antibody. A mouse antibody to β-actin (1:5,000; Sigma-Aldrich) or a rabbit antibody to GAPDH (1:1,000; Cell Signaling Technology) was used for control experiments. The blots were developed with Super Script West Pico Chemoluminescent Substrate Kit according to the manufacturer's procedures (ThermoScientific).

Cell cycle analysis by flow cytometry. For cell cycle analysis, K562 stable pools were collected by centrifugation, resuspended in PBS containing 3.75% Nonidet P-40, 100 µg/ml RNase A and 40 µg/ml propidium iodide, and incubated at room temperature for 3 h in the dark. Samples were analyzed on a FACScan flow cytometer (Becton Dickinson Immunocytometry Systems, BDIS). The cell cycle analysis was performed in triplicate with the program ModFit LT3.0.

Microscopic analysis of K562 stable pools. K562 cells and K562 stable pools were fixed with 4% paraformaldehyde and centrifuged on cytospin slides. Cytospin slides were stained by hematoxylin-eosin. Cells fixed were stained by 1 µg/ml DAPI and analyzed with a Zeiss axiovert 200M microscope equipped with a plan-apochromat 63×/1.4 oil immersion objective. The size of nuclei major and minor axes were measured in pixels on DAPI images acquired by the Zeiss axiovert 200M microscope. Numbers of nuclei analyzed were as follows: 18 nuclei for PSM2 stable pool, 19 for nonsilencing shRNAmir stable pool and 28 for SEC23B silencing stable pool.

Morpholino microinjection into zebrafish. We injected phosphorodiamidate morpholino oligomers (morpholinos; Gene Tools) into wild-type Tü strain embryos at the 1- to 2-cell stage using a Harvard PLI-100 Pico-Injector (Holliston). For morpholino sequences, see **Supplementary Table 5**.

RT-PCR of zebrafish RNA. Total RNA from 3 d.p.f. wild-type and morphant larvae was prepared with TRIzol reagent (Invitrogen). Traces of genomic DNA were removed by DNase-1 RNAse free digestion (Roche). Comparable amounts of total RNA were subjected to reverse transcription with oligo-dT primers, by using SuperScript III Reverse Transcriptase (Invitrogen) according to the manufacturer's instructions. PCR conditions wereas follows: 98 °C × 3 min; 98 °C ×15 s, 62 °C × 30 s, 72 °C × 90 s for 35 cycles; followed by 10 min extension at 72 °C. For cDNA primer sequences, see **Supplementary Table 5**.

Analysis of zebrafish erythrocytes. For zebrafish blood collection, larvae at 3 d.p.f. were placed in lateral decubitus in a solution containing 0.9× PBS,

doi:10.1038/ng.405

1% BSA, 0.0002% heparin and 0.02% buffered solution of Tricaine methanesulfonate (MS222). We severed tails using a razor blade and collected blood cells using a P20 pipettman. Blood cells were transferred into chilled Eppendorf tubes containing 0.9× PBS and 1% BSA. Cells were pelleted in a microcentrifuge (100*g*, 10 min), resuspended in 300 µl 0.9× PBS and 1% BSA and cytospun onto glass slides. Slides were Wright-Giemsa stained, and cells were counted under light microscopy.

For protein blot of zebrafish erythrocytes, antisera directed against 14 C-terminal amino acid residues (C-LDADDANVKFDDED) of zebrafish band3 (also called anion exchanger 1, Slc4a1 and AE1) were generated in rabbits and affinity-purified against the immunizing peptides (Genemed Synthesis)[30]. Hsp60 antibody (sc-1722), goat anti-rabbit IgG-HRP (cat. no. sc-2054) and donkey anti-goat IgG-HRP (sc-2020) are from Santa Cruz. We lysed and denatured 1× PBS buffer-washed embryonic erythrocytes from control and Sec23b morphant embryos of 3 d.p.f. with 1 volume of 2× Laemmli SDS sample buffer (Biorad) under two conditions: 65 °C 10 min and 95 °C 5 min. Protein samples were separated on 10% acrylamide gels and transferred on Immun-Blot PVDF membrane (Biorad). The membranes were probed using antibody to band3 (1:5,000) with peroxidase-conjugated goat antibody to rabbit IgG (Santa Cruz) as the secondary antibody (1:3,000). As a loading control, membranes were re-probed using antibody to hsp60 (1:500) with donkey antibody to goat IgG (Santa Cruz) as the secondary antibody (1:3,000). The chemiluminescent method was used for detection (SuperSignal West Pico Substrate, Pierce).

SEC23B structure. The model of human SEC23B was generated with MODELLER[31] on the basis of the crystal structure of human SEC23A (protein data bank code 2NUT).

FACS analysis of fibroblasts. We carried out multicolor flow cytometry using a BD FacsAria with Diva 6.1 Software. For each antigen analyzed, fluorochrome-coupled antibodies were used acording to the manufacturer's protocols (antibodies are available on request); as negative control, corresponding fluorochrome-coupled isotypes were applied. GPI-anchored proteins were detected with FLAER (Protox Biotech). PBS was used as a control for FLAER. The fluorescence intensity of 100,000 cells was acquired.

Fibroblast differentiation assays. Adipogenic (Lonza), chondrogenic and osteogenic (Miltenyi Biotech) differentiation of fibroblasts were performed according to the manufacturers' protocols.

Reagents for cell biology studies. Cycloheximide was from Calbiochem, anti-SEC23 and anti-SEC23B sera were from Abcam, anti-Calnexin was from Stressgene, anti-SEC31, anti-GM130 and anti-EEA1 were from BD Biosciences, anti-Lamp1 (H4A3) was obtained from Developmental Studies Hybridoma Bank, University of Iowa, anti-β-COP was described elsewhere[32] and anti-ts-O45-G monoclonal antibody 'VG' recognizing an extra-cellular epitope of the CFP-tagged vesicular stomatitis virus glycoprotein ts-O45-G was a gift from K. Simons (Max Planck Institute of Molecular Cell Biology and Genetics). Recombinant adenovirus encoding the cargo marker protein ts-O45-G tagged with CFP was described[33]. Silencer siRNA duplexes against SEC23 were from Ambion with the following siRNA identification numbers: 17796 (siSEC23A-1), 17702 (siSEC23A-2), 17795 (siSEC23B-1) and 17882 (siSEC23B-2). The sequence of the control siScramble duplex is listed in **Supplementary Table 5**.

Cell culture and microinjection. HeLa-Kyoto cells (human cervix carcinoma cells), a gift from S. Narumiya (Kyoto University) and T. Hirota (Institute of Molecular Pathology, Vienna, Austria), and control as well as F4P1 fibroblasts were maintained in DMEM (Life Technologies) supplemented with 10% FCS, 1% penicillin and streptomycin, and 1% glutamine in a 37 °C humidified incubator with 5% CO_2. For microinjection or immunostaining, cells were grown on life cell dishes (MatTEk) or Lab-Tek II Chambered coverglass (Nunc) or on 15-mm coverslips. Cells were microinjected using an Eppendorf microinjection system as previously described[32]. Injection markers were used at a concentration of 0.4 mg/ml.

Transport assays. Cells were plated onto coverslips and siRNA transfections were performed following the manufacturer's recommendations using oligofectamine. At 24 h after transfection, cells were infected with the CFP-ts-O45-G-adenovirus and incubated at the nonpermissable temperature 39.5 °C and 5% CO_2 for 16 h. To release the CFP-tagged ts-O45-G from the ER, we placed the coverslips in a 32 °C water bath for 60 min followed by fixation.

Immunostaining. HeLa Kyoto cells, control and F4P1 fibroblasts were fixed either with 100% methanol at −20 °C for 4 min or with 3% PFA for 20 min at room temperature. PFA-treated cells were subsequently treated with 3% glycine in PBS for 5 min and permeabilized with 0.1% Triton X-100 in PBS for an additional 5 min. Fixed and permeabilized cells were incubated with primary antibodies in PBS for 30 min. Samples were washed three times for 5 min in PBS and then incubated for 30 min in Alexa-568 conjugated anti-rabbit or anti-mouse secondary antibodies, and finally washed three times for 5 min in PBS. Cells grown on coverslips were mounted on glass slides with Mowiol. Cells grown on live cell dishes were left in PBS. All images were processed and quantified using NIH ImageJ.

URLs. Assay manual, https://www.affymetrix.com/support/downloads/manuals/100k_manual.pdf.

26. Crookston, J.H., Crookston, M.C. & Rosse, W.F. Red-cell abnormalities in HEMPAS (hereditary erythroblastic multinuclearity with a positive acidified-serum test). *Br. J. Haematol.* **23** (Suppl.), 83–91 (1972).
27. Ronzoni, L. *et al.* Erythroid differentiation and maturation from peripheral CD34+ cells in liquid culture: cellular and molecular characterization. *Blood Cells Mol. Dis.* **40**, 148–155 (2008).
28. Chomczynski, P. & Sacchi, N. Single-step method of RNA isolation by acid guanidiniumthiocyanate-phenol-chloroform extraction. *Anal. Biochem.* **162**, 156–159 (1987).
29. Livak, K.J. & Schmitteng, T.D. Analysis of relative gene expression data using real-time quantitative PCR and the 2(−ΔΔC(T)). *Methods* **25**, 402–408 (2001).
30. Paw, B.H. *et al.* Cell-specific mitotic defect and dyserythropoiesis associated with erythroid band3 deficiency. *Nat. Genet.* **34**, 59–64 (2003).
31. Eswar, N., Eramian, D., Webb, B., Shen, M.Y. & Sali, A. Protein structure modeling with MODELLER. *Methods Mol. Biol.* **426**, 145–159 (2008).
32. Pepperkok, R. *et al.* Beta-COP is essential for biosynthetic membrane transport from the endoplasmic reticulum to the Golgi complex in vivo. *Cell* **74**, 71–82 (1993).
33. Keller, P., Toomre, D., Diaz, E., White, J. & Simons, K. Multicolour imaging of post-Golgi sorting and trafficking in live cells. *Nat. Cell Biol.* **3**, 140–149 (2001).